TRIANGULAR COSSERAT POINT ELEMENT METHOD FOR REDUCING SOFT TISSUE ARTIFACT: VALIDATION AND APPLICATION TO GAIT

A Thesis

presented to

the Faculty of California Polytechnic State University,

San Luis Obispo

In Partial Fulfillment

of the Requirements for the Degree

Master of Science in Mechanical Engineering

by

Jake Edward Deschamps

December 2021

COMMITTEE MEMBERSHIP

TITLE:	Triangular Cosserat Point Element Method for Reducing Soft Tissue Artifact: Validation and Application to Gait
AUTHOR:	Jake Edward Deschamps
DATE SUBMITTED:	December 2021
COMMITTEE CHAIR:	Stephen Klisch, Ph.D. Professor of Mechanical Engineering
COMMITTEE MEMBER:	Scott Hazelwood, Ph.D. Professor of Biomedical Engineering
COMMITTEE MEMBER:	William R. Murray, Ph.D. Professor of Mechanical Engineering

ABSTRACT

Triangular Cosserat Point Element Method for Reducing Soft Tissue Artifact: Validation and Application to Gait

Jake Edward Deschamps

Human motion capture technology is a powerful tool for advancing the understanding of human motion biomechanics (Andriacchi and Alexander, 2000). This is most readily accomplished by applying retroreflective markers to a participant's skin and tracking the position of the markers during motion. Skin and adipose tissue move independently of the underlying bone during motion creating error known as soft tissue artifact (STA), the primary source of error in human motion capture (Leardini et al., 2005).

(Solav et al., 2014) proposed and (Solav et al., 2015) expanded the triangular Cosserat point element (TCPE) method to reduce the effect of STA on derived kinematics through application of a marker cluster analyzed as a set of triangular Cosserat point elements. This method also provides metrics for three different modes of STA.

Here the updated TCPE method (Solav et al., 2015) was compared to the established point cluster (PC) method of (Andriacchi et al., 1998) and the marker position error minimizing Procrustes solution (PS) method of (Söderkvist and Wedin, 1993) in two implant-based simulations, providing quantitative measures of error, and standard gait analysis, providing qualitative comparisons of each method's determined kinematics. Both of these experiments allowed the TCPE method to generate observed STA parameters, informing the efficacy of the simulation.

The TCPE method's performance was similar to the PS method's in the implant simulations and in standard gait. The PC method's results seemed to be affected by numerical instability: simulation trial errors were larger and standard gait results were only similar to the other methods' in general terms. While the PS and TCPE results were comparable, the TCPE method's physiological basis provided the added benefit of non-rigid behavior quantization through its STA parameters. In this study, these parameters were on the same order of

magnitude between the standard gait experiments and the simulations, suggesting that implant simulations could be valuable substitutes when invasive methods are not available.

Keywords: Human Motion Biomechanics, Motion Analysis, Gait Analysis, Soft Tissue Artifact

ACKNOWLEDGMENTS

This work was supported by the Donald E. Bently Center for Engineering Innovation (SMK); Cal Poly's Solutions Through Research in Diet and Exercise (STRIDE) Center (JED); Quartus Engineering Inc. (JED); and the Defense Health Program, through the Department of Defense Broad Agency Announcement for Extramural Medical Research Program #W81XWH-BAA-14-1 under Award No. W81XWH-16-1-0051. Opinions, interpretations, conclusions and recommendations are those of the author and are not necessarily endorsed by the Department of Defense.

I would like to thank my committee chair, Dr. Stephen Klisch, for providing me with the tremendous opportunity to help found the Human Motion Biomechanics Lab through the setup required for these experiments. Your positivity and optimism gave me the determination that I needed to see this project through. Your help focusing the goals of this project was instrumental in maintaining a reasonable scope. If the reader wishes to know the degree to which this was valuable, know that many of the suggestions I have included for future experiments and projects were things that I had wanted to add to this one.

I would also like to thank my parents, Kate and Vin Deschamps. I would never have had the opportunity to receive such a fantastic education had it not been for them. My father's drive and strong will were particularly essential throughout this process, giving me an example that I aspire to emulate.

Lastly, I would like to thank Brianna Morrison, my significant other throughout this process. Thank you so much for your bountiful support, and for helping with proofreading drafts as well.

TABLE OF CONTENTS

Page

LIST OF TABLES…. viii
LIST OF FIGURES ix
CHAPTER
1. INTRODUCTION 1
2. METHODS 3
2.1 Motion Capture System 3
2.2 Marker Position Recording 3
2.3 Implementation of Algorithms 3
2.4 TCPE Method 3
2.4.1 Obtaining Strain, Rotation, and Translation 4
2.4.2 TCPE Filtering Parameters and Selection 6
2.5 PC and PS Methods 8
2.6 Human Experiment Protocols 9
2.7 Validation Experiments 9
2.7.1 Pendulum Validation Experiment 9
2.7.2 Gait Plate Validation Experiment 11
2.8 Standard Gait Experiments 12
2.9 Quantization of STA 13
3. RESULTS 14
4. DISCUSSION 19
REFERENCES 24
APPENDICES
A. Right Stretch Tensor Determination 26
B. Rotation Averaging 26
C. Conversion from Rotation Matrix to Axis—Angle Representation 26
D. Pendulum Angle Determination and Decomposition 27
E. Gait Plate Angle Decomposition 28
F. Knee Angles: Rotation Application and Decomposition 29

LIST OF TABLES

Table Page

1. Numerical rotational RMS error for all methods.....15

2. Summary of vectors used during knee angle determination.....31

LIST OF FIGURES

Figure Page

1. Pendulum apparatus fitted with implant and markers ... 9
2. Gait plate on participant fitted with extension rod, implant, and markers ... 11
3. Rotational RMS error by experiment and by component ... 14
4. Translational RMS error by experiment and by component ... 15
5. Free and impact swing angles of select trials ... 16
6. Average gait kinematics by participant and by component ... 17
7. Average TCPE strain ... 18
8. Average TCPE rotational deviation ... 18
9. Average TCPE translational deviation ... 18

Chapter 1
INTRODUCTION

Human motion capture is an established technology with numerous applications, including the potential to combine observed kinematic motion with measured kinetic forces to estimate stress within joints during physical activity (Andriacchi and Alexander, 2000). These systems use cameras to record the three-dimensional positions of retroreflective markers attached to a participant. Software analysis subsequently processes these marker trajectories in an attempt to determine the motion of the underlying bone. Markers may be mounted directly to a participant's bones; however, this process is both invasive and expensive (Benoit et al., 2006; Tashman et al., 2007). Mounting markers to a participant's skin with an adhesive greatly improves the accessibility of this technology, but presents another issue: the efficacy of these surface marker applications hinges upon the ability to reconstruct the motion of underlying bone from the motion of the skin.

Skin and adipose tissue frequently move independently of a person's bone structure. This movement creates error known as soft tissue artifact (STA). STA is a primary source of error in human motion capture (Leardini et al., 2005). Commonly used clinical methods, like the Helen Hayes method, consider individual segments of the body to be rigid, and all observed marker motion is taken as indicative of bone motion. Errors caused by STA can significantly alter the measured kinematics of many human motions. (Reinschmidt et al., 1997) observed that erroneous rotation from STA could be almost as large as the true motion for knee varus/valgus and internal/external rotations. The importance of understanding STA can readily be seen in the sheer volume of studies conducted to document its modes, measure its magnitudes, and develop techniques to reduce its effects. As such, it has been well established that STA is a significant challenge that clinical motion capture laboratories must contend with.

The central focus of this study is a relatively recent technique developed in (Solav et al., 2014; Solav et al., 2015) to reduce the effect of STA on body segment kinematics. This method models segments using triangular Cosserat point elements (i.e., deformable bodies that can experience homogenous deformations). It characterizes STA using physiologically relevant

parameters and attempts to isolate rigid motion. Previous methods, like the point cluster (PC) method of (Andriacchi et al., 1998) and the Procrustes solution (PS) method of (Söderkvist and Wedin, 1993), have used mathematical optimization techniques to reduce the effect of STA. This triangular Cosserat point element (TCPE) method, however, uses continuum mechanics to treat the body segment as capable of deformation.

The goals of this study were three-fold: 1) validate the implementation of the TCPE method using STA simulations with known motion, 2) apply the TCPE method to knee angle determination during human gait, and 3) compare the performance of the TCPE method with established methods.

Chapter 2
METHODS

2.1. Motion Capture System

A motion capture laboratory with eight cameras, Cortex software (OWL digital camera system, Cortex V5.0, Motion Analysis Corp., Santa Rosa, CA, USA), walkway/force plate (AMTI, Watertown, MA, USA) and analog-to-digital converter (Texas Instruments, Dallas, TX, USA) were used. Marker data was collected at 60 Hz, interpolated (third-order spline), and filtered (4^{th}-order Butterworth, 6 Hz cutoff).

2.2. Marker Position Recording

A global coordinate system was defined for the room in which experiments took place. This consisted of an origin and a right-handed set of three orthonormal base vectors ($\hat{\boldsymbol{e}}_1$, $\hat{\boldsymbol{e}}_2$, and $\hat{\boldsymbol{e}}_3$) that functioned as coordinate axes. Each point in the room could be described by its distance from the origin in each component direction. The motion capture system recorded the positions of markers within this coordinate system 60 times every second. Each instant at which these positions were recorded is called a frame, in reference to the motion capture camera system's framerate.

2.3. Implementation of Algorithms

All equations, procedures, and algorithms described in the subsequent sections were implemented in MATLAB software (MATLAB R2020a, The MathWorks, Inc., Natick, MA, USA), with the exception of a reduced form of the TCPE method used for identifying standard error in STA parameters which was implemented in Octave software (GNU Octave Version 6.3.0, The Octave Project Developers).

2.4. TCPE Method

A cluster of at least six markers was placed on each non-rigid body being analyzed (the implant, the thigh, the shank). Fewer markers were used for rigid bodies (the pendulum, the plate). All possible combinations of three markers were analyzed as TCPEs. The dynamics of the body were characterized by this group of TCPEs.

A reference configuration was defined and captured for each body. The selection of the reference configuration differed for each experiment (see relevant subsections), but the body was static in each case when possible. The TCPE method determined transformations that mapped each TCPE from its reference configuration to each frame of motion.

2.4.1. Obtaining Strain, Rotation, and Translation

The following equations use direct notation (in which vectors and tensors are denoted by a bold font) or, when additional clarity is needed, indicial notation with $i, j, k, A = 1, 2, 3$ (in which repeated indices use the summation convention except when noted). The reference positions of the three markers of the TCPE under analysis are indicated by the vectors $\boldsymbol{X}_1$, $\boldsymbol{X}_2$, and $\boldsymbol{X}_3$ while the present positions are represented by $\boldsymbol{x}_1$, $\boldsymbol{x}_2$, and $\boldsymbol{x}_3$. All equations appear in (Solav et al., 2014; Solav et al., 2015) or are standard.

Directors, special vectors formulated to provide some information about deformation (Rubin, 1985), were determined for each TCPE in the reference configuration and in the present configuration. The first two directors were obtained with vector subtraction, while the third was obtained by normalizing the cross product of the other two through division by its magnitude. The vector magnitude is denoted with vertical bars as |·|. The calculations for the present configuration are shown below. Those for the reference configuration follow the same formulation. The aforementioned usage of uppercase letters for the reference configuration and lowercase letters for the present configuration extends to the directors as well.

$$\boldsymbol{d}_1 = \boldsymbol{x}_1 - \boldsymbol{x}_3 \qquad \boldsymbol{d}_2 = \boldsymbol{x}_2 - \boldsymbol{x}_3 \qquad \boldsymbol{d}_3 = \frac{\boldsymbol{d}_1 \times \boldsymbol{d}_2}{|\boldsymbol{d}_1 \times \boldsymbol{d}_2|} \tag{1}$$

The reference configuration directors were then used to define reciprocal reference configuration directors as follows:

$$\boldsymbol{D}^1 = \frac{\boldsymbol{D}_2 \times \boldsymbol{D}_3}{|\boldsymbol{D}_1 \times \boldsymbol{D}_2|} \qquad \boldsymbol{D}^2 = \frac{\boldsymbol{D}_3 \times \boldsymbol{D}_1}{|\boldsymbol{D}_1 \times \boldsymbol{D}_2|} \qquad \boldsymbol{D}^3 = \frac{\boldsymbol{D}_1 \times \boldsymbol{D}_2}{|\boldsymbol{D}_1 \times \boldsymbol{D}_2|} \tag{2}$$

The reference configuration reciprocal directors and the present configuration directors then yielded the deformation gradient tensor as below in direct notation (in which ⊗ represents the tensor product) and in indicial notation:

$$\boldsymbol{F} = \boldsymbol{d}_1 \otimes \boldsymbol{D}^1 + \boldsymbol{d}_2 \otimes \boldsymbol{D}^2 + \boldsymbol{d}_3 \otimes \boldsymbol{D}^3$$
$$F_{iA} = d_{1i} D^{1A} + d_{2i} D^{2A} + d_{3i} D^{3A} \quad (3)$$

In this equation, the first index on each director refers to the specific director. The second index refers to the component of the director. For example, d_{11}, d_{12}, and d_{13} are the components of $\boldsymbol{d}_1$ in the $\hat{\boldsymbol{e}}_1$, $\hat{\boldsymbol{e}}_2$, and $\hat{\boldsymbol{e}}_3$ directions respectively. The first term in the above equation multiplies the i^{th} component of the first director in the present configuration with the A^{th} component of the first reciprocal reference configuration director.

This deformation gradient tensor was of critical interest as it brings the TCPE from its reference configuration to its present configuration. The TCPE's rotation tensor, Lagrangian strain tensor, and translation vector were all derived from this deformation gradient tensor in the following process.

The deformation gradient tensor was first manipulated to obtain the Right Cauchy-Green deformation tensor.

$$\boldsymbol{C} = \boldsymbol{F}^T \boldsymbol{F} \quad (4)$$

The square root of this tensor was taken to obtain the right stretch tensor. This process utilized eigenvalue decomposition further detailed in Appendix A.

$$\boldsymbol{U} = \boldsymbol{C}^{1/2} \quad (5)$$

The rotation tensor describing the rotation of the TCPE was then found using the inverse of the Right stretch tensor.

$$\boldsymbol{R} = \boldsymbol{F}\boldsymbol{U}^{-1} \quad (6)$$

The Lagrangian strain tensor was then determined using the Right Cauchy-Green deformation tensor. In this equation, $\boldsymbol{I}$ represents the 3×3 identity matrix.

$$\boldsymbol{E} = \frac{1}{2}(\boldsymbol{C} - \boldsymbol{I}) \quad (7)$$

Translations were obtained for each TCPE using the following approach, as detailed in (Solav et al., 2015). The position of each TCPE's centroid in the reference and present configurations was determined by taking the mean of the three component markers' positions.

$$\bar{\boldsymbol{X}} = \frac{1}{3}(\boldsymbol{X}_1 + \boldsymbol{X}_2 + \boldsymbol{X}_3) \qquad \bar{\boldsymbol{x}} = \frac{1}{3}(\boldsymbol{x}_1 + \boldsymbol{x}_2 + \boldsymbol{x}_3) \tag{8}$$

The centroid's positions were used in combination with the deformation gradient tensor to determine the translation of a specific key point. This key point moved rigidly with the underlying body and was particular to each experiment. This particular point's position in the reference configuration is referred to below as $\boldsymbol{X}^{(B)}$. The translation $\boldsymbol{t}^{(B)}$ of this point from its reference to its present position was determined as follows:

$$\boldsymbol{t}^{(B)} = \bar{\boldsymbol{x}} - \boldsymbol{F}\left(\bar{\boldsymbol{X}} - \boldsymbol{X}^{(B)}\right) - \boldsymbol{X}^{(B)} \tag{9}$$

This equation allows the key point's translation to be determined even when its position is not readily available in the present configuration. The validity of this expression is demonstrated in the short proof below which introduces the present key point position as $\boldsymbol{x}^{(B)}$.

$$\begin{aligned} \boldsymbol{t}^{(B)} &= \bar{\boldsymbol{x}} - \boldsymbol{F}\left(\bar{\boldsymbol{X}} - \boldsymbol{X}^{(B)}\right) - \boldsymbol{X}^{(B)} \\ \boldsymbol{t}^{(B)} &= \bar{\boldsymbol{x}} - \left(\bar{\boldsymbol{x}} - \boldsymbol{x}^{(B)}\right) - \boldsymbol{X}^{(B)} \\ \boldsymbol{t}^{(B)} &= \bar{\boldsymbol{x}} - \bar{\boldsymbol{x}} + \boldsymbol{x}^{(B)} - \boldsymbol{X}^{(B)} \\ \boldsymbol{t}^{(B)} &= \boldsymbol{x}^{(B)} - \boldsymbol{X}^{(B)} \end{aligned} \tag{10}$$

In a perfectly rigid case, multiplying the deformation gradient tensor with the position of the key point relative to the TCPE centroid in the reference frame generates that same relative position in the present frame. Thus, the centroid terms disappear and only the difference between the present and reference key point positions remains.

2.4.2. TCPE Filtering Parameters and Selection

The above process was repeated to obtain a Lagrangian strain magnitude, rotation tensor, and key point translation for each TCPE. Specific elements were then selected according to filtering parameters based on strain, rotational variation, and translational variation.

Lagrangian strain magnitude characterized each element's deformation. Under rigid motion, this parameter would be zero. It was calculated as follows for the J^{th} TCPE, with $tr(\cdot)$ representing the matrix trace.

$$|\boldsymbol{E}|_J = \sqrt{tr\left(\boldsymbol{E}_J \boldsymbol{E}_J^T\right)} \tag{11}$$

Rotational variations between the J^{th} and K^{th} TCPEs were calculated as follows. If these TCPEs experienced identical rotations, then this value would be zero.

$$\phi_{J/K} = \cos^{-1}\left[\frac{1}{2}\left\{tr\left(\boldsymbol{R}_J\boldsymbol{R}_K^T\right) - 1\right\}\right] \tag{12}$$

This parameter was then averaged across K to determine the average rotational variation for the J^{th} TCPE as follows. Note that there is no need to ignore the case where $J = K$, as $\phi_{J/J} = 0$.

$$\phi_J = \frac{1}{N_{TCPE} - 1}\sum_{K=1}^{N_{TCPE}} \phi_{J/K} \tag{13}$$

The method described in (Solav et al., 2014) was expanded in (Solav et al., 2015) to include translational variation. This was initially calculated between the J^{th} and K^{th} TCPEs using:

$$T_{J/K} = \left|\boldsymbol{t}_J{}^{(B)} - \boldsymbol{t}_K{}^{(B)}\right| \tag{14}$$

If both TCPEs determined the same translation, this value would also be zero. As with the rotational variation parameter, these were then averaged across K to give each TCPE a mean translational variation. As before, there is no need to ignore the case in which $J = K$.

$$T_J = \frac{1}{N_{TCPE} - 1}\sum_{K=1}^{N_{TCPE}} T_{J/K} \tag{15}$$

The strain magnitude, rotational variation, and translational variation were each normalized to span the range $[0, 1]$.

$$N_J^E = \frac{|\boldsymbol{E}|_J - |\boldsymbol{E}|_{min}}{|\boldsymbol{E}|_{max} - |\boldsymbol{E}|_{min}} \qquad N_J^{\Delta\phi} = \frac{\phi_J - \phi_{min}}{\phi_{max} - \phi_{min}} \qquad N_J^{\Delta T} = \frac{T_J - T_{min}}{T_{max} - T_{min}} \tag{16}$$

A final combined filtering parameter was then obtained by averaging the three parameters for each TCPE.

$$N_J{}^{comb} = \frac{1}{3}\left(N_J^E + N_J^{\Delta\phi} + N_J^{\Delta T}\right) \tag{17}$$

This final filtering parameter dictated TCPE selection. All TCPEs with a combined filtering parameter less than or equal to 0.1 were selected. If fewer than three TCPEs met this criterion, the three TCPEs with the lowest combined filtering parameters were selected.

The rotation tensors of the selected TCPEs were then averaged through a process detailed in (Markley et al., 2007) and summarized in Appendix B. Briefly, this process determined

an average rotation tensor minimizing the difference between each rotation matrix and this average, as given by the square of the Frobenius norm. This procedure differs from that which was employed in (Solav et al., 2014).

$$\bar{\boldsymbol{R}} = \arg\min_{\boldsymbol{R}\in SO(3)} \sum_{i=1}^{n} \|\boldsymbol{R} - \boldsymbol{R}_i\|_F^2 \tag{18}$$

The values of $|\boldsymbol{E}|_J$, ϕ_J, T_J were recorded for each TCPE on each frame, and were separately averaged to create average strain, average rotational variation, and average translational variation for each experiment (Refer to the "Quantization of STA" subsection).

2.5. PC and PS Methods

Two established marker cluster-based methods were implemented for comparison: the point cluster (PC) method developed by (Andriacchi et al., 1998) and the Procrustes solution (PS) method developed by (Söderkvist and Wedin, 1993). Both of these methods determine a rigid body rotation while treating the cluster as effectively rigid. The PC method adjusts marker weight values to reduce changes to a representative inertia matrix and the PS method determines rotations to minimize marker position error.

The PC method first created an inertia matrix for the cluster by assigning each marker a weight value, with all markers taking the same value in the reference configuration. These weight values were then used to formulate an inertia tensor treating each marker as a point mass. These individual marker weights were then adjusted at each frame to minimize changes to this inertia matrix, as measured by changes to its eigenvalues. The rotation matrix was then obtained by leveraging the eigenvectors of this inertia matrix.

The PS method analyzed the cluster by minimizing overall marker position error. This error was determined by comparing the recorded position of each marker with a position determined through application of a single rigid body translation and rotation to the cluster's reference configuration. The minimization of the sum of the squares of these errors was analyzed as a variation of the Procrustes problem and solved through singular value decomposition.

The PS method was selected to provide translation results. Instability observed with the PC method in this study and others such as (Cereatti et al., 2006) discounted the implementation

of translation for this method in favor of emphasizing the comparison between the PS and TCPE methods.

The PC and PS methods used the same reference configurations as the TCPE method when determining transformations between the reference and present configurations.

2.6. Human Experiment Protocols

Experimental protocols were approved by Cal Poly's Human Subjects Committee and were designed to minimize risk to human participants. Participants included four healthy, male individuals aged 20-24 with body mass index ranging from 21.8-26.4 and no history of leg injury.

2.7. Validation Experiments

2.7.1. Pendulum Validation Experiment

This experiment was conducted to validate the TCPE method in the most controlled physical setting possible. As in (Solav et al., 2014), a silicone implant was fixed to the end of a rigid pendulum simulating a system of soft tissue and rigid bone, shown in Figure 1.

Figure 1. Pendulum apparatus fitted with implant and markers

The pendulum's structure was outfitted with four markers: one on each end of the rotation axis, one approximately halfway down the length of the pendulum, and another at the end of the pendulum. The TCPE method then attempted to determine the rotation of the rigid pendulum and the translation of the marker at the end of the pendulum from the motion of a cluster of seven markers placed on the implant. The PC and PS methods also determined rotations for comparison; the PS method determined translations as well. Error was determined quantitatively, as the true motion of the pendulum was known.

Each trial began with the pendulum at rest in its lowest position. This static position provided the reference configuration for the pendulum and the implant during the trial. The pendulum was then manually raised and released. During free swing trials, the pendulum was allowed to swing uninterrupted. During impact swing trials, the pendulum's motion was momentarily halted as it approached its initial point of release.

The true angle of the pendulum was first determined by defining five vectors using marker pairs. These vectors were then projected onto the plane of swing and compared at each frame with their reference configuration counterparts. This process is further detailed in Appendix D. The results of this vector solution were compared to angles obtained by applying the TCPE method to the pendulum markers. Once these had been determined to be suitably consistent, the TCPE-derived rigid pendulum angles were used, as in (Solav et al., 2014).

Rotations determined by each cluster-based method were converted into axis—angle representation using a process detailed in Appendix C and separated into three components about a set of axes that rotated with the pendulum. These components were: about the pendulum's axis of rotation, about the long axis of the pendulum, and about the cross product of the previous two. This process is further detailed in Appendix D.

Root-mean-square (RMS) errors were determined for each method in each component of rotation and for translations determined by the TCPE and PS methods.

2.7.2. Gait Plate Validation Experiment

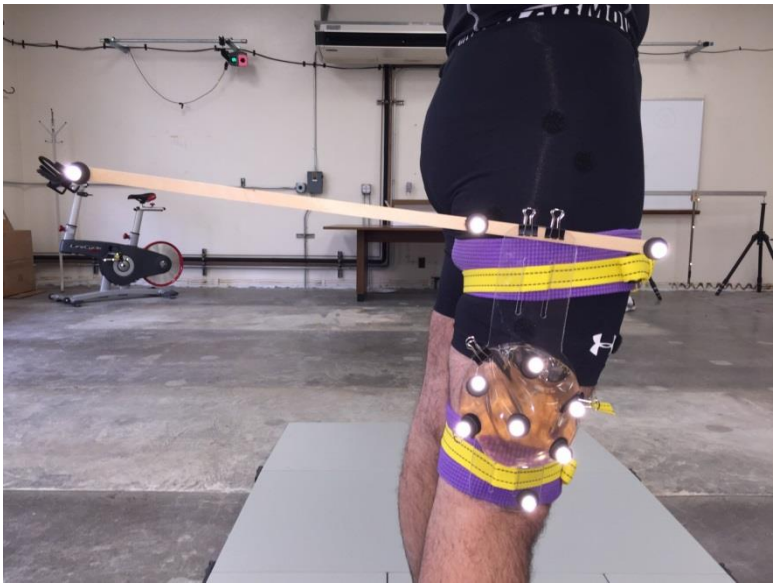

Figure 2. Gait plate on participant fitted with extension rod, implant, and markers

A rigid plate and extension rod assembly was affixed to a participant's thigh, shown in Figure 2. This plate was then outfitted with markers to determine its true motion. Three markers were placed along the extension rod and another was placed below the implant, close to the participant's knee. The implant was connected to the side of the plate and equipped with six markers. As in the pendulum experiment, the TCPE method determined the angle of the plate and the translation of a key point (the lower plate marker) based on the trajectories of the implant markers. The PC and PS methods also analyzed the implant markers to determine rotation for comparison, with the PS method determining key point translation as well.

This experiment improved upon the pendulum validation through the use of gait as the driving motion. The pendulum experiment enabled testing each method in a controlled, one-dimensional case. Its rotations were largely sinusoidal, with interruptions from simulated impacts. This plate experiment tested each method on three-dimensional physiological motion with heel strike induced impacts. The accuracy of each method could be directly determined as the true underlying motion of the plate was still known. This informed each method's ability to process the complex motion of the thigh, better illustrating their ability to determine knee kinematics.

Dynamic trials were challenging to capture due to marker adhesion issues. As such, only one trial was successfully taken, featuring the participant crossing the room at a self-selected walking speed. This adhesion issue also prevented the successful capture of a static pose reference configuration. As such, one frame from this trial (just before heel strike) was used as the reference configuration.

For the purposes of RMS error calculation, marker-derived and true angles were converted into axis–angle representation using a process detailed in Appendix C. These angles were decomposed as described in Appendix E. RMS errors were then calculated for each component on each frame. True angles were determined using three plate markers (extension front, extension rear, plate low) as a single TCPE.

2.8. Standard Gait Experiments

Standard gait experiments were conducted with three participants to compare knee kinematics obtained with the cluster-based marker systems. These systems used a seven-marker cluster on the right thigh and another seven-marker cluster on the right shank. The participants were also outfitted with the Helen Hayes (HH) marker set consisting of the following 19 markers (symmetric where relevant): toes, heels, lateral and medial malleoli, lateral and medial femoral condyles, anterior superior iliac spine, sacrum, and asymmetric offset markers on the thigh and shank. The HH marker set shared the asymmetric offset markers on the participant's right side with markers from the cluster-based set. Implementation of the HH marker set allowed Cortex software to determine HH-derived knee kinematics for each trial, and the functional joint centers (FJCs) of the hip, knee, and ankle. While not used for comparison, the HH-derived kinematics were used to identify and isolate the gait cycle. The FJCs were used to form the basis for knee angle decomposition. The TCPE and PS methods also used the knee FJC location as their key point for translation determination.

After a static pose capture, medially placed markers were removed so as not to interfere with the participant's normal gait. The participant walked across the room many times at a self-selected speed until at least five trials had occurred where the participant impacted the force plate with their right foot during a natural gait cycle.

Each trial was normalized to encompass one gait cycle. This cycle began with the right foot contacting the force plate and ended with the next right foot impact, as determined by a local flexion minimum in Cortex's determined kinematics. The time-scale was then transformed to percent of gait cycle: from 0% (right heel strike) to 100% (next right heel strike). This normalization technique enabled averaging of multiple trials for the same participant and comparisons across participants.

Helen Hayes marker locations acquired during the static pose capture along with Cortex-determined functional joint centers were used to determine vectors representing the thigh and shank. The rotations determined by each cluster-based method were applied to these vectors, giving present thigh and shank orientations. Knee angles were then determined from these representative vectors using a method consistent with the floating axis system developed in (Wu and Cavanagh, 1995). The initial definition of these vectors and the details of this method are included in Appendix F.

2.9. Quantization of STA

Application of the TCPE method to each experiment generated three filtering parameters for each TCPE for each frame: a strain parameter, a rotational variation parameter, and a translational variation parameter. These filtering parameters were direct results of non-rigid behavior and would be zero in the presence of perfectly rigid motion. Each parameter was averaged across all TCPEs and all frames for each experiment, creating three metrics indicating the level of non-rigid behavior present in each. These metrics were then compared across experiments to inform the efficacy of the implant based simulation.

Chapter 3

RESULTS

For both validation experiments, RMS errors were very similar for the TCPE and PS methods. Figure 3 and Figure 4 show these errors were within less than half a degree of rotation or a millimeter of translation in many cases. In some translation cases, the difference was slightly greater than a millimeter, though neither method appears evidently superior. Rotational RMS errors were the lowest about the primary axis of rotation for each experiment. For the pendulum validation, this was about the pendulum's swing axis. For the gait plate validation, this was about the motion capture system's y-axis, which roughly corresponded to rotation within the sagittal plane.

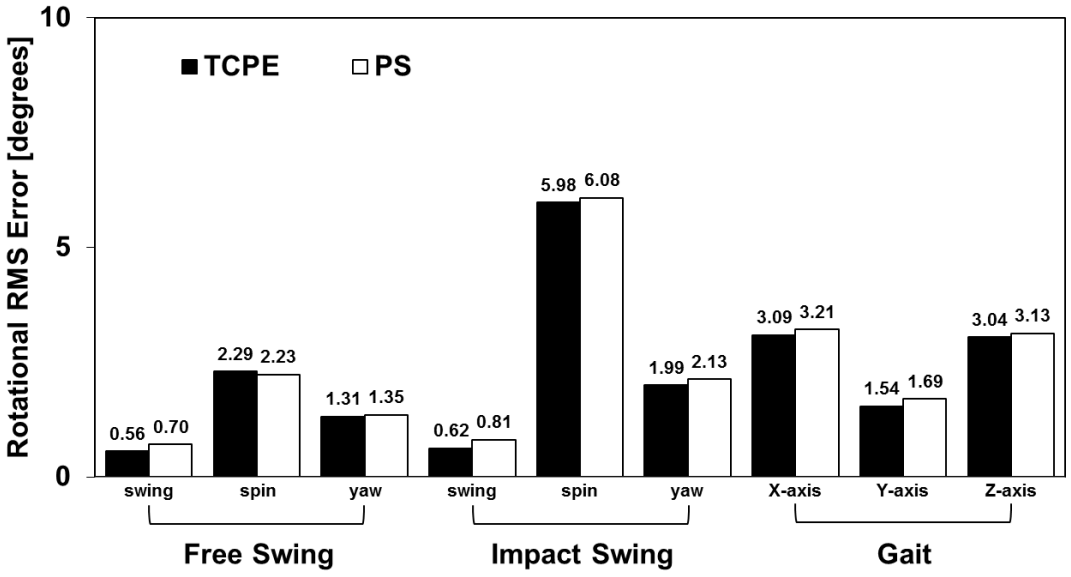

Figure 3. Rotational RMS error by experiment and by component

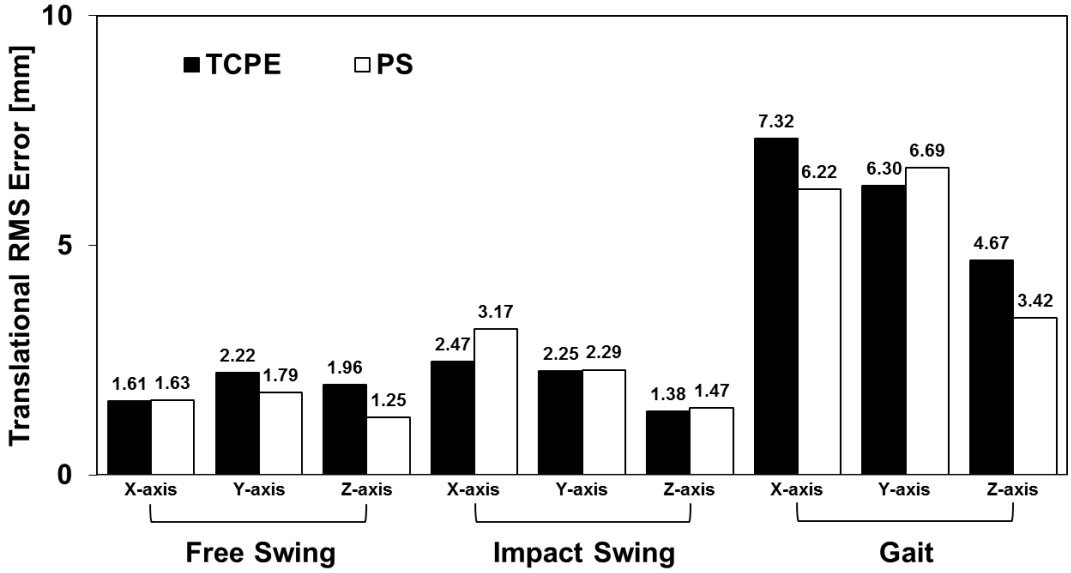

Figure 4. Translational RMS error by experiment and by component

The PC method's RMS errors were generally substantially higher. These results are omitted from the figures above and instead presented in Table 1. Rotational RMS errors associated with the TCPE and PS methods during the pendulum trial were low compared with the range of motion. For the TCPE method, errors about the primary axis of rotation were just 0.66% of the range of motion for the free swing trials and 0.78% for the impact swing trials. For the PS method, these values were 0.82% and 1.03%, respectively. Rotational RMS error compared with the range of motion was similarly low for these methods about the motion capture system's y-axis during the gait simulation: 3.30% for the TCPE method and 3.62% for the PS method. Rotation about this axis roughly corresponded to rotation within the sagittal plane.

Table 1. Numerical rotational RMS error for all methods

	Rotational RMS Error [degrees]								
	Free Swing			Impact Swing			Gait		
	Swing	Spin	Yaw	Swing	Spin	Yaw	X-axis	Y-axis	Z-axis
TCPE	0.56	2.29	1.31	0.62	5.98	1.99	3.09	1.54	3.04
PC	2.30	3.48	3.95	3.25	7.33	6.50	10.34	11.22	34.41
PS	0.70	2.23	1.35	0.81	6.08	2.13	3.21	1.69	3.13

Determined kinematics for the pendulum trials were similar for the TCPE and PS methods in the swing component, as shown in Figure 5. Results for these methods closely

followed the true motion. Results determined by the PC method were generally similar, but showed large, instantaneous deviations from the true motion, most notably during impact trials.

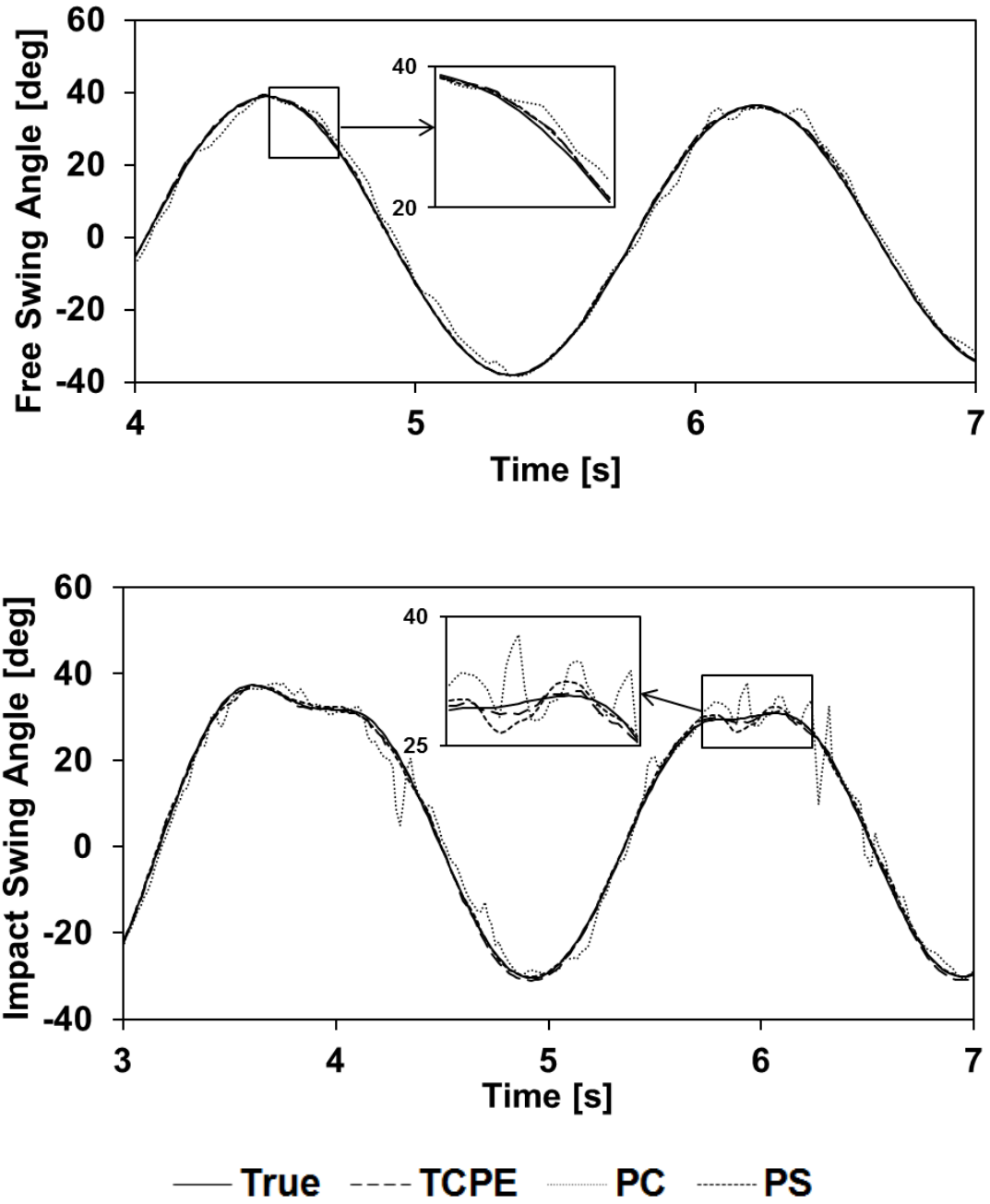

Figure 5. Free and impact swing angles of select trials

The TCPE and PS methods also showed similar kinematic trends for the standard gait experiment, shown in Figure 6 with a vertical line indicating toe-off. As with the pendulum experiments, the PC results were generally similar, but with large, instantaneous deviations from the results of the other methods. These PC results have been omitted for visual clarity.

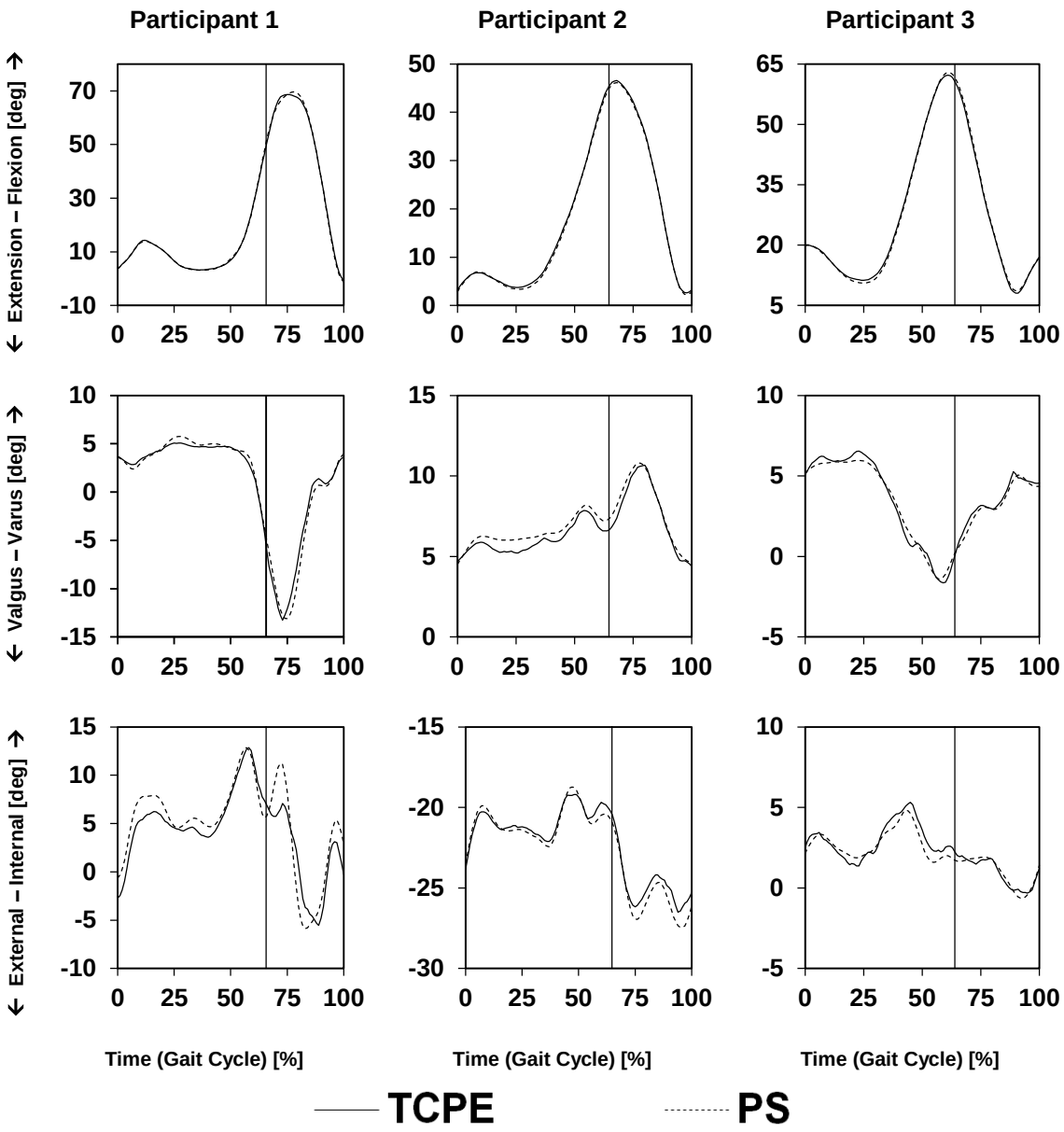

Figure 6. Average gait kinematics by participant and by component

All three of the TCPE filtering parameters (strain, rotational variation, translational variation) had the same order of magnitude through the validation and the standard gait experiments, as shown in Figure 7, Figure 8, and Figure 9.

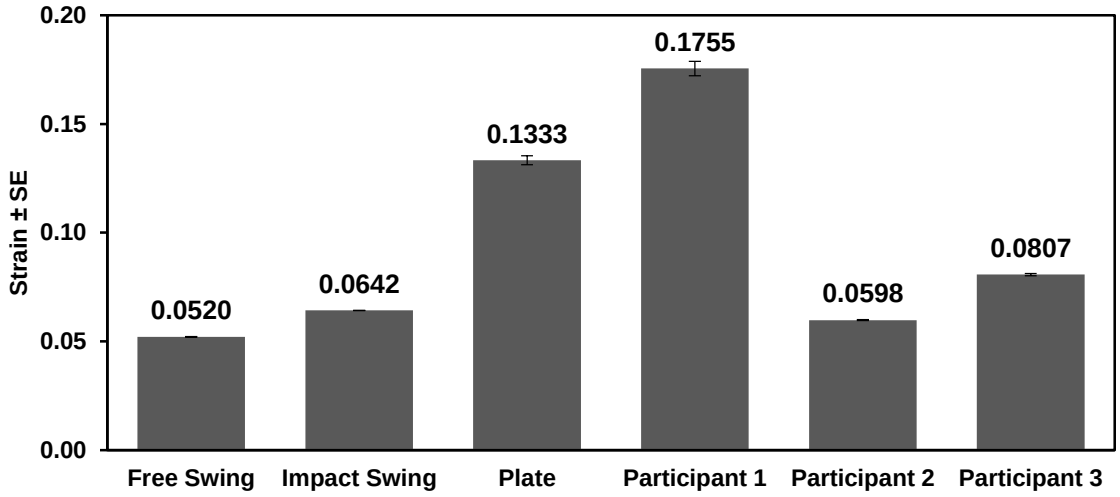

Figure 7. Average TCPE strain

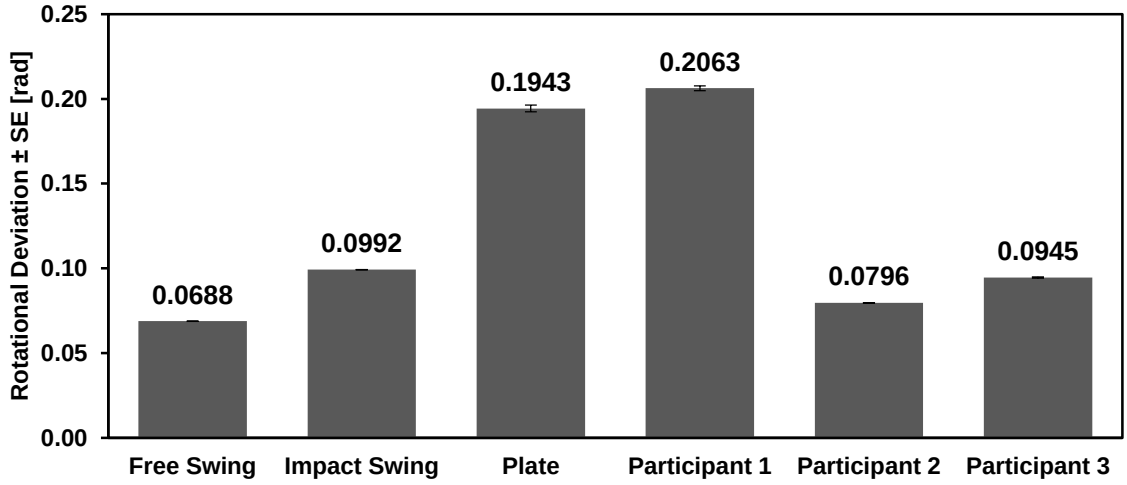

Figure 8. Average TCPE rotational deviation

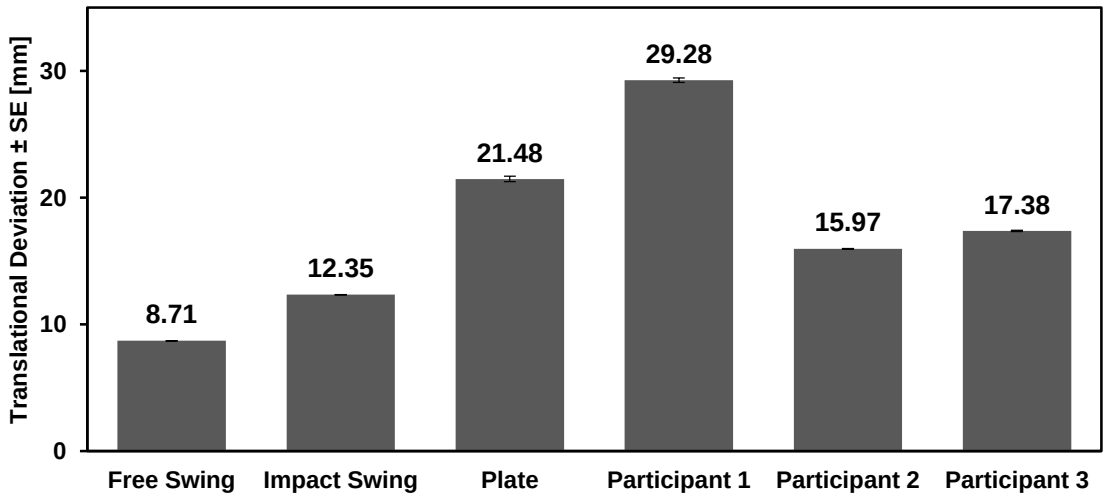

Figure 9. Average TCPE translational deviation

Chapter 4
DISCUSSION

The first objective of this study was to validate the TCPE method's ability to reduce STA in controlled applications. This objective was fulfilled by the pendulum validation, which extended the one-dimensional analysis of (Solav et al., 2014) to three dimensions, and the gait validation. The error found in both of these experiments was low compared to the range of motion about the primary axis of rotation. In (Cappozzo et al., 1996), the differences between true shank motion during walking and those determined using surface markers had RMS values from 1.0 degrees to 3.5 degrees depending on the component and marker combination, with an average of 3.0 degrees. The RMS errors observed with the TCPE method's results about the swing axis of the pendulum and the y-axis of the motion capture system were both below this value. Therefore, the error introduced by the simulated STA was sufficiently mitigated to obtain reasonably accurate kinematics.

The second objective was to apply the TCPE method to the determination of knee angles during human gait. The knee angles determined for the three participants analyzed were qualitatively consistent with results obtained by the PS method and those obtained in many other studies (Baudet et al., 2014; Rivest, 2005; Schache et al., 2006; LaFortune et al., 1992) in which the most consistent trend was the presence of two characteristic local flexion maxima. The first of these occurred during early stance. The second occurred near toe-off and was substantially larger. Kinematics for varus/valgus and internal/external rotations vary considerably across studies and participants, so drawing conclusions for these components would require more participants.

The third objective was to contrast the performance of the TCPE method with the more established PC (Andriacchi et al., 1998) and PS (Söderkvist and Wedin, 1993) methods. This was done in both validations and standard gait experiments. The TCPE and PS methods had very similar measures of error in the validation experiments. The error present in the PC method's

validation results was significantly higher. The knee kinematics in the standard gait experiments were also qualitatively similar for the TCPE and PS methods in all participants.

The magnitudes of all three TCPE method filtering parameters found in the validation experiments had the same order of magnitude as those found in the standard gait experiments. This suggests that the amounts of the three modes of STA the implant experienced were comparable to that of the thigh and shank of the human participants. This supports the validation study conducted here as the implant may be taken as having adequately simulated physiological levels of STA in terms of resulting strain, rotational variation, and translational variation. Additionally, it suggests that implant-based simulations may prove to be viable alternatives to invasive methods for future studies focused on the effectiveness of STA reducing algorithms.

These STA parameters are one of the most compelling aspects of the TCPE method. These parameters can provide many insights. Much of the data that has been gathered for gait is for adult male participants. As additional studies are conducted using other demographics, these STA parameters may help inform the differences and unique challenges of capturing kinematics for each group. These may also help identify the relative STA present for individuals of differing BMIs and during other activities, such as pitching a baseball, running, or cycling. With enough development, the STA parameters could potentially be used to determine rough statistical confidence intervals for motion capture data in lieu of gold-standard measurements for a particular experiment.

While the PC method's determined kinematics followed the same general trajectory during the validation and gait experiments, they contained a large amount of instantaneous angle variations. This occurred even during the free swinging portion of the pendulum's motion when the true angle of the pendulum was changing gradually. These characteristics were likely indicative of numerical instability, as was observed in (Cereatti et al., 2006). More recent PC studies have used clusters of 10 or 11 markers (Dyrby and Andriacchi, 2004; Scanlan et al., 2010), while the marker clusters present in this study contained seven or fewer. As a result, conclusions made regarding the relative accuracy of the PC method must be made with caution.

This may be viewed as evidence that the TCPE and PS methods are favorable in situations where using larger numbers of markers is not feasible.

This study used seven markers for the gait and pendulum trials following the procedure outlined in (Solav et al., 2014). A future study could explore the accuracy of each method as the number of markers in each cluster is changed. Using greater numbers of markers would likely increase the quality of the determined kinematics, but the practicality of using more markers in a cluster depends on the application. Marker misidentification can occur if large numbers of markers are placed in a compact area, lengthening the amount of time needed to obtain and process motion capture data regardless of the method chosen. This issue led to using only six markers on the implant during the gait plate simulation, and obtaining only one usable trial even with this reduction. Knowing each method's performance at certain marker numbers could be valuable information when designing an experiment.

Given the general similarity in the quality of the PS and TCPE methods' results, it is worthwhile elaborating on the differences between the two methods. The PS method is, at its core, a method of mathematical optimization. Despite this, it is not an iterative process and only entails the singular value decomposition of a 3×3 matrix and other more basic matrix arithmetic operations. The TCPE method is similarly non-iterative, primarily consisting of computationally inexpensive steps. Still, the TCPE method is likely more intensive as much of its algorithm must be repeated for each triangular element. Its analysis becomes lengthier as more markers are added to a cluster. The number of triangular elements within a cluster of n markers is given by the number of combinations of three markers that can be formed, ${}_nC_3$. This value grows rapidly as more markers are added. Contrasting improvements to accuracy provided by additional markers with the practical challenges of implementing such markers is a subject for another study, as previously mentioned.

A critical difference between the PS and TCPE methods is that of optimization versus filtering. The PS method determines rigid transformations that, when applied to the cluster, minimize the difference between the observed and the determined positions of *all* markers. The TCPE method uses physiological parameters to filter out marker triangles that were more

significantly affected by STA, and is therefore capable of using only select markers to identify the final rotation and translation at each instant. A future study could use simulated marker trajectories to contrast each method's performance when an intentionally erroneous marker is introduced. This could illuminate the TCPE method's potential to filter out troublesome markers and indicate their effect on the PS method's optimization. This contrast may prove particularly important when anticipating analysis of more extreme motions, such as pitching a baseball or running.

The TCPE method's physiological basis provides another significant difference. The PS method approaches non-rigid motion on a per-marker basis, reducing its representation to one that is more akin to measurement error. The TCPE method treats each triangle of three markers as a deformable body, characterizing its deformation and using these parameters to select triangles that were least affected by STA. The difference between these approaches may appear subtle. The TCPE method uses physiological metrics to describe the cluster's STA, and then uses the most rigid portions of the cluster while the PS method assumes the entire cluster to be rigid and finds the most suitable transformations given this assumption.

There are several additional ways in which this study may be expanded and improved. The gait plate validation presented here used only a single plate for the thigh. Thus, the rotations of the plate could only be interpreted in an arbitrary, non-anatomical coordinate system. Implementing a second plate for the shank would allow for the determination of simulated knee angles, deepening the understanding of the TCPE method's ability to reduce the effect of STA on determined knee angles and illuminating the potentially compounding effect that the STA of the thigh and shank may have. The texture and size of the implant posed issues for markers, both in number and adhesion. Placing larger numbers of markers on this limited surface created issues for the motion capture system's marker identification, and, whenever a marker lost adhesion with the implant's surface, the trial had to be restarted. This was remedied by increasing the number of trials recorded, and by manually cleaning the data; however, a larger surface area for marker placement and better marker adhesion would enable obtaining more usable validation trials within

the period of access to the participant. These issues also posed a limitation on the number of markers that could be placed on the implant, prohibiting tests with larger marker clusters.

Impact trials for the pendulum experiment had large amounts of spin about the pendulum itself. As the implant's rotation around the pendulum itself was unconstrained, this likely represented true motion of the implant. A future implementation may consider using a circular piece of rigid material behind the implant to constrain this motion. Similarly, the largest component of rotational motion for the gait plate experiment was about the motion capture system's z-axis, indicating that the plate apparatus was likely able to rotate about the participant's thigh during motion. A future study may take this into consideration when developing a new method of attaching the plate to the participant.

Finally, a future study could include a gold-standard method, such as MRI. (Solav et al., 2015) only implemented bone pin markers for the thigh, so true knee angles could not be determined. Full implementation of gold standard derived kinematics would greatly help the assessment of the TCPE determined knee kinematics.

REFERENCES

Andriacchi, T.P., Alexander, E., Toney, M., Dyrby, C., Sum, J., 1998. A point cluster method for in vivo motion analysis: applied to a study of knee kinematics. Journal of Biomechanical Engineering 120, 743—749.

Andriacchi, T.P., Alexander, E., 2000. Studies of human locomotion: past, present and future. Journal of Biomechanical Engineering 33(10), 1217—1224.

Baudet, A., Morisset, C., d'Athis, P., Maillefert, J.-F., Casillas, J.-M., Ornetti, P., Laroche, D., 2014. Cross-Talk Correction Method for Knee Kinematics in Gait Analysis Using Principal Component Analysis (PCA): A New Proposal. PloS one 9, 1932—6203.

Belongie, S., 2012. Rodrigues' Rotation Formula. From MathWorld, A Wolfram Web Resource, created by Eric W. Weisstein. http://mathworld.wolfram.com/RodriguesRotationFormula.html.

Benoit, D.L., Ramsey, D.K., Lamontagne, M., Xu, L., Wretenberg, P., Renström, P., 2006. Effect of skin movement artifact on knee kinematics during gait and cutting motions measured in vivo. Gait & Posture 24, 152—164.

Cappozzo, A., Catani, F., Leardini, A., Benedetti, M.G., Croce, U.D., 1996. Position and orientation in space of bones during movement: experimental artefacts. Clinical Biomechanics 11(2), 90—100.

Cereatti, A., Della Croce, U., Cappozzo, A., 2006. Reconstruction of skeletal movement using skin markers: comparative assessment of bone pose estimators. Journal of neuroengineering and rehabilitation 3(1), 1743—0003.

Dyrby, C.O., Andriacchi, T.P., 2004. Secondary motions of the knee during weight bearing and non-weight bearing activities. Journal of Orthopaedic Research 22, 794—800.

Leardini, A., Chiari, L., Della Croce, U., Cappozzo, A., 2005. Human movement analysis using stereophotogrammetry: Part 3. Soft tissue artifact assessment and compensation. Gait & posture 21, 212—225.

LaFortune, M.A., Cavanagh, P.R., Sommer, H.J., Kalenak, A., 1992. Three-dimensional kinematics of the human knee during walking. Journal of Biomechanics 25, 347—357.

Markley, F.L., Cheng, Y., Crassidis, J. L., Oshman, Y., 2007. Averaging quaternions. Journal of Guidance, Control, and Dynamics 30(4), 1193—1197.

quat2rotm. n.d. In *MathWork's MATLAB documentation* (2020a). Retrieved from https://www.mathworks.com/help/robotics/ref/quat2rotm.html.

Reinschmidt C., van den Bogert A.J., Lundberg A., Nigg B.M., Murphy N., Stacoff A., Stano A., 1997. Tibiofemoral and tibiocalcaneal motion during walking: external vs. skeletal markers. Gait & Posture 6, 98—109.

Rivest, L.-P., 2005. A correction for axis misalignment in the joint angle curves representing knee movement in gait analysis. Journal of biomechanics 38, 1604—1611.

rotm2quat. n.d. In *MathWork's MATLAB documentation* (2020a). Retrieved from https://www.mathworks.com/help/robotics/ref/rotm2quat.html.

Rubin, M. B., 1985. On the Theory of a Cosserat Point and Its Application to the Numerical Solution of Continuum Problems. Journal of Applied Mechanics 52(2), 368—372.

Scanlan, S.F., Chaudhari, A.M., Dyrby, C.O., Andriacchi, T.P., 2010. Differences in tibial rotation during walking in ACL reconstructed and healthy contralateral knees. Journal of Biomechanics 43, 1817—1822.

Schache, A.G., Baker, R., Lamoreux, L.W., 2006. Defining the knee joint flexion–extension axis for purposes of quantitative gait analysis: an evaluation of methods. Gait & Posture 24, 100—109.

Söderkvist, I., Wedin, P.-Å., 1993. Determining the movements of the skeleton using well-configured markers. Journal of biomechanics 26, 1473—1477.

Solav, D., Rubin, M., Wolf, A., 2014. Soft Tissue Artifact compensation using Triangular Cosserat Point Elements (TCPEs). International Journal of Engineering Science 85, 1—9.

Solav, D., Rubin, M.B., Cereatti, A., Camomilla, V., Wolf, A., 2015. Bone Pose Estimation in the Presence of Soft Tissue Artifact Using Triangular Cosserat Point Elements. Annals of biomedical engineering, 1—10.

Tashman, S., Kolowich, P., Collon, D., Anderson, K., Anderst, W., 2007. Dynamic function of the ACL-reconstructed knee during running. Clinical orthopaedics and related research 454, 66—73.

Wu, G., Cavanagh, P.R., 1995. ISB recommendations for standardization in the reporting of kinematic data. Journal of Biomechanics 28, 1257—1261.

APPENDICES

A. Right Stretch Tensor Determination

The square root of the right Cauchy-Green deformation tensor was required to determine the right stretch tensor $\boldsymbol{U}$, repeated below.

$$\boldsymbol{U} = \boldsymbol{C}^{1/2}$$

This was carried out by employing eigenvalue decomposition, shown in the following equation. A_i represents the eigenvalues of $\boldsymbol{C}$. $\boldsymbol{V}_i$ represents the respective eigenvectors, in column format.

$$\boldsymbol{U} = \left(A_1^{\frac{1}{2}}\right)\boldsymbol{V}_1 \otimes \boldsymbol{V}_1 + \left(A_2^{\frac{1}{2}}\right)\boldsymbol{V}_2 \otimes \boldsymbol{V}_2 + \left(A_3^{\frac{1}{2}}\right)\boldsymbol{V}_3 \otimes \boldsymbol{V}_3 \tag{19}$$

B. Rotation Averaging

Average rotation tensors were determined using the method described in (Markley et al., 2007), summarized here. The following procedure minimizes the sum of the squared Frobenius norms of the differences between each of the n rotation tensors and the average. This minimization is characterized by the following equation, repeated from section 2.4.2.

$$\bar{\boldsymbol{R}} = \arg\min_{\boldsymbol{R} \in SO(3)} \sum_{i=1}^{n} \|\boldsymbol{R} - \boldsymbol{R}_i\|_F^2$$

All n rotation tensors were transformed to their quaternion representation using MATLAB's built-in function ("rotm2quat"). These quaternions were expressed in column form, with the vector part occupying the first three components and the scalar part occupying the fourth. A new matrix M was then determined with the following:

$$\boldsymbol{M} = \sum_{i=1}^{n} \boldsymbol{q}_i \otimes \boldsymbol{q}_i \text{ (no summation implied for index i)} \tag{20}$$

The average quaternion was then the eigenvector of M that corresponded with the largest eigenvalue. This quaternion was then converted back to a rotation matrix using MATLAB's built-in function ("quat2rotm").

C. Conversion from Rotation Matrix to Axis—Angle Representation

The conversion from a rotation tensor $\boldsymbol{R}$ to axis—angle representation was used repeatedly in the following sections. It was carried out according to the following formula, consistent with Rodrigues' theorem (Belongie, 2012).

Axis—angle representation consists of rotation by an angle θ about an axis $\boldsymbol{e}$. First, the angle was determined using the trace of the rotation tensor.

$$\theta = \cos^{-1}\left(\frac{1}{2}(tr(\boldsymbol{R}) - 1)\right) \tag{21}$$

The components of the rotation axis were then determined using this angle and specific elements of the rotation tensor.

$$\boldsymbol{e} = \frac{1}{2\sin\theta}\begin{bmatrix} R_{32} - R_{23} \\ R_{13} - R_{31} \\ R_{21} - R_{12} \end{bmatrix} \tag{22}$$

The obtained axis and angle were used to determine the magnitudes of rotation in each component direction through scalar multiplication of the angle and axis.

D. Pendulum Angle Determination and Decomposition

D1. Vector Solution for True Pendulum Angle

The true angle for the pendulum was preliminarily determined using a vector solution. First, the axis of rotation for the pendulum was determined using the markers on the front ($\boldsymbol{m}_f$) and back ($\boldsymbol{m}_b$) of the pendulum's axis.

$$\boldsymbol{a} = \boldsymbol{m}_b - \boldsymbol{m}_f \tag{23}$$

This value was determined for all frames of motion. In each subsequent equation in which $\boldsymbol{a}$ appears, it should be taken that $\boldsymbol{a}$ was obtained using the relevant frame.

Reference vectors were created from the first frame of the capture, prior to displacing the pendulum. These vectors were created between each of the following pairs of markers: the front of the axis to the middle of the pendulum ($\boldsymbol{m}_m$), the back of the axis to the middle of the pendulum, the front of the axis to the end of the pendulum ($\boldsymbol{m}_e$), the back of the axis to the end of the pendulum, and the middle of the pendulum to the end of the pendulum. The rejection of these vectors from $\boldsymbol{a}$ was used to create vectors that were entirely in the plane of rotation.

$$\boldsymbol{v}_{f-m} = \boldsymbol{m}_f - \boldsymbol{m}_m - \frac{(\boldsymbol{m}_f - \boldsymbol{m}_m)\cdot\boldsymbol{a}}{|\boldsymbol{a}|^2}\boldsymbol{a}$$

$$\boldsymbol{v}_{b-m} = \boldsymbol{m}_b - \boldsymbol{m}_m - \frac{(\boldsymbol{m}_b - \boldsymbol{m}_m)\cdot\boldsymbol{a}}{|\boldsymbol{a}|^2}\boldsymbol{a}$$

$$\boldsymbol{v}_{f-e} = \boldsymbol{m}_f - \boldsymbol{m}_e - \frac{(\boldsymbol{m}_f - \boldsymbol{m}_e) \cdot \boldsymbol{a}}{|\boldsymbol{a}|^2} \boldsymbol{a} \tag{24}$$

$$\boldsymbol{v}_{b-e} = \boldsymbol{m}_b - \boldsymbol{m}_e - \frac{(\boldsymbol{m}_b - \boldsymbol{m}_e) \cdot \boldsymbol{a}}{|\boldsymbol{a}|^2} \boldsymbol{a}$$

$$\boldsymbol{v}_{m-e} = \boldsymbol{m}_m - \boldsymbol{m}_e - \frac{(\boldsymbol{m}_m - \boldsymbol{m}_e) \cdot \boldsymbol{a}}{|\boldsymbol{a}|^2} \boldsymbol{a}$$

These vectors were determined for each frame of motion as well, creating present vectors. The angle between the reference and present versions of each vector gave the angle of the pendulum according to the following equation.

$$\theta = \cos^{-1}\left(\frac{\boldsymbol{v}_{reference} \cdot \boldsymbol{v}_{present}}{|\boldsymbol{v}_{reference}||\boldsymbol{v}_{present}|}\right) \tag{25}$$

Since the pendulum swung in the yz-plane, sign was determined by comparing the y-components of the vector in the reference and present frames. Finally, the angles determined from each pair of vectors were averaged to determine the pendulum's rigid-body angle.

D2. Pendulum Angle Decomposition

The pendulum rotation angles were decomposed into components according to a set of axes rotating with the pendulum. These axes were defined as the following: about the pendulum's rotation axis ($\boldsymbol{a}$, determined in the previous section), about the pendulum itself (determined by averaging all variations of $\boldsymbol{v}$ described in the previous section, taking the rejection with $\boldsymbol{a}$, and then normalizing), and about the cross product of the previous axes.

Implant derived angles were decomposed into these components on each frame. This was done by converting the rotation matrices derived by the cluster-based methods into axis—angle representation. The dot product of this axis—angle representation was then taken with each component unit vector to determine the portion of the rotation that was in the corresponding direction.

E. Gait Plate Angle Decomposition

In lieu of anatomical context, plate angles were determined based on the room coordinate system. Converting each rotation into axis—angle representation allowed for swift decomposition according to the room's set of three orthonormal base vectors ($\hat{\boldsymbol{e}}_1$, $\hat{\boldsymbol{e}}_2$, and $\hat{\boldsymbol{e}}_3$).

F. Knee Angles: Rotation Application and Decomposition

F1. Representative Vector Formulation

Vectors representing the positions of the thigh and shank were formed. The HH markers were used to determine the positions of the thigh and shank during the reference frame, due to their placement over bony prominences. Given the static nature of the reference frame, these marker locations were particularly accurate. The virtual FJC markers generated during the static trial were also employed in this process. The coordinates of the virtual marker at the hip joint center, $\boldsymbol{H}_c$, and the coordinates of the virtual marker at the knee joint center, $\boldsymbol{K}_c$, were used to create a unit vector defining the thigh.

$$\widehat{\boldsymbol{T}} = \frac{\boldsymbol{K}_c - \boldsymbol{H}_c}{|\boldsymbol{K}_c - \boldsymbol{H}_c|} \tag{26}$$

This one vector could not fully define the orientation of the thigh, so a perpendicular vector was defined. The position of the lateral femoral epicondyle, represented by $\boldsymbol{E}_l$ and the position of the medial femoral epicondyle marker, represented by $\boldsymbol{E}_m$, were used for this purpose.

$$\widehat{\boldsymbol{T}}_p = \frac{\widehat{\boldsymbol{T}} \times (\boldsymbol{E}_m - \boldsymbol{E}_l)}{\left|\widehat{\boldsymbol{T}} \times (\boldsymbol{E}_m - \boldsymbol{E}_l)\right|} \tag{27}$$

The same process was used to create functionally similar vectors for the shank. The ankle joint center, $\boldsymbol{A}_c$, and the knee joint center, $\boldsymbol{K}_c$, yielded the shank unit vector $\widehat{\boldsymbol{S}}$**.**

$$\widehat{\boldsymbol{S}} = \frac{\boldsymbol{A}_c - \boldsymbol{K}_c}{|\boldsymbol{A}_c - \boldsymbol{K}_c|} \tag{28}$$

The shank's perpendicular vector, $\widehat{\boldsymbol{S}}_p$, was determined using the medial and lateral malleoli, $\boldsymbol{M}_m$ and $\boldsymbol{M}_l$, respectively.

$$\widehat{\boldsymbol{S}}_p = \frac{\widehat{\boldsymbol{S}} \times (\boldsymbol{M}_m - \boldsymbol{M}_l)}{\left|\widehat{\boldsymbol{S}} \times (\boldsymbol{M}_m - \boldsymbol{M}_l)\right|} \tag{29}$$

F2. Transformation to the Present Frame

Cluster-based methods determined rotation matrices for each frame describing the transformation from the reference configuration to the present configuration for each segment. The thigh's rotation matrix,$\boldsymbol{R}_t$, and the shank's rotation matrix, $\boldsymbol{R}_s$, were applied to the thigh and

shank vectors, $\widehat{\boldsymbol{T}}$, $\widehat{\boldsymbol{T}}_p$, $\widehat{\boldsymbol{S}}$, and $\widehat{\boldsymbol{S}}_p$, to yield unit vectors that indicated the present orientation of the thigh and shank.

$$\hat{\boldsymbol{t}} = \boldsymbol{R}_t \widehat{\boldsymbol{T}} \tag{30}$$

$$\hat{\boldsymbol{t}}_p = \boldsymbol{R}_t \widehat{\boldsymbol{T}}_p \tag{31}$$

$$\hat{\boldsymbol{s}} = \boldsymbol{R}_s \widehat{\boldsymbol{S}} \tag{32}$$

$$\hat{\boldsymbol{s}}_p = \boldsymbol{R}_s \widehat{\boldsymbol{S}}_p \tag{33}$$

F3. Anatomical Knee Angle Determination

The three anatomical knee angles, consistent with (Wu and Cavanagh, 1995), were determined for the standard gait experiments according to the following procedure. Of primary use during this analysis were the present configuration unit vectors representing the thigh and the shank, as well as their respective perpendicular vectors. These were obtained according to the procedures described in the previous appendices. Both the thigh and shank vectors pointed inferiorly; both the perpendicular vectors were directed anteriorly.

These three anatomical knee angles were defined as follows:

- Flexion was defined as the angle between the thigh and shank in the sagittal plane of the thigh. Flexion was positive when the shank was posterior of the thigh.
- Varus rotation was defined as the angle between the thigh and shank in the frontal plane of the thigh. Varus rotation was positive when the shank was medial of the thigh.
- Internal rotation was defined as the remaining rotation about the axis of the shank. Internal rotation was positive when the participant's shank was rotated medially from its forward position.

A brief summary of the vectors used during this procedure is shown in Table 2. Also note that many of the following equations include the magnitudes of unit vectors and other operations that do not affect the end result. These are included here to maintain consistency with general vector equations, and may be omitted due to their unitary values.

Table 2. Summary of vectors used during knee angle determination

$\hat{\boldsymbol{t}}$—Unit vector representing the thigh	$\boldsymbol{r}$—Rejection of the shank onto the thigh	θ_v—Angle of varus rotation.
$\hat{\boldsymbol{s}}$—Unit vector representing the shank	$\boldsymbol{r}_f$—Projection of $\boldsymbol{r}$ onto the flexion axis, $\hat{\boldsymbol{f}}$	θ_f—Angle of flexion.
$\hat{\boldsymbol{t}}_p$—Thigh's perpendicular vector	$\boldsymbol{r}_p$—Projection of $\boldsymbol{r}$ onto the thigh's perpendicular vector, $\hat{\boldsymbol{t}}_p$	θ_i—Angle of internal rotation.
$\hat{\boldsymbol{s}}_p$—Shank's perpendicular vector	$\hat{\boldsymbol{t}}_f$—Thigh that has been rotated by the flexion angle about $\hat{\boldsymbol{f}}$	$\hat{\boldsymbol{t}}_{pf}$—Perpendicular vector for $\hat{\boldsymbol{t}}_f$
$\hat{\boldsymbol{f}}$—Flexion axis, defined as $\boldsymbol{f} = \hat{\boldsymbol{t}} \times \hat{\boldsymbol{t}}_p$	$\hat{\boldsymbol{s}}_v$—Shank that has had its varus rotation undone.	$\hat{\boldsymbol{t}}_{pfv}$—Thigh's perpendicular that has had flexion and varus rotations applied. Note $\hat{\boldsymbol{t}}_{pfv} = \hat{\boldsymbol{t}}_{pf}$

F3.1. Varus Rotation

F3.1.1. Determining Varus Rotation Magnitude

The rejection of one vector onto another (in this case the shank $\hat{\boldsymbol{s}}$ onto the thigh $\hat{\boldsymbol{t}}$) is given by:

$$\boldsymbol{r} = \hat{\boldsymbol{s}} - \frac{\hat{\boldsymbol{s}} \cdot \hat{\boldsymbol{t}}}{\hat{\boldsymbol{t}} \cdot \hat{\boldsymbol{t}}} \hat{\boldsymbol{t}} \tag{34}$$

This expression can be rewritten as:

$$\frac{\hat{\boldsymbol{s}} \cdot \hat{\boldsymbol{t}}}{\hat{\boldsymbol{t}} \cdot \hat{\boldsymbol{t}}} \hat{\boldsymbol{t}} = \hat{\boldsymbol{s}} - \boldsymbol{r}$$

If we define two more vectors ($\boldsymbol{r}_f$ – the projection of $\boldsymbol{r}$ onto the flexion axis, and $\boldsymbol{r}_p$, the projection of $\boldsymbol{r}$ onto the thigh's perpendicular vector), we can see that these two vectors form a plane perpendicular to $\hat{\boldsymbol{t}}$, and thus encompass the entirety of $\boldsymbol{r}$. So, from the first equation:

$$\boldsymbol{r}_f + \boldsymbol{r}_p = \hat{\boldsymbol{s}} - \frac{\hat{\boldsymbol{s}} \cdot \hat{\boldsymbol{t}}}{\hat{\boldsymbol{t}} \cdot \hat{\boldsymbol{t}}} \hat{\boldsymbol{t}}$$

$\boldsymbol{r}_f$ can also be expressed as a vector rejection of the shank onto a shank that has had its varus motion undone:

$$\boldsymbol{r}_f = \hat{\boldsymbol{s}} - |\hat{\boldsymbol{s}}| \cos\theta_v \, \hat{\boldsymbol{s}}_v$$

Subtracting this equation from the previous one:

$$\boldsymbol{r}_f + \boldsymbol{r}_p - \boldsymbol{r}_f = \hat{\boldsymbol{s}} - \frac{\hat{\boldsymbol{s}} \cdot \hat{\boldsymbol{t}}}{\hat{\boldsymbol{t}} \cdot \hat{\boldsymbol{t}}} \hat{\boldsymbol{t}} - \hat{\boldsymbol{s}} + |\hat{\boldsymbol{s}}| \cos \theta_v \, \hat{\boldsymbol{s}}_v$$

Simplifying:

$$\boldsymbol{r}_p = -\frac{\hat{\boldsymbol{s}} \cdot \hat{\boldsymbol{t}}}{\hat{\boldsymbol{t}} \cdot \hat{\boldsymbol{t}}} \hat{\boldsymbol{t}} + |\hat{\boldsymbol{s}}| \cos \theta_v \, \hat{\boldsymbol{s}}_v$$

$$\boldsymbol{r}_p + \frac{\hat{\boldsymbol{s}} \cdot \hat{\boldsymbol{t}}}{\hat{\boldsymbol{t}} \cdot \hat{\boldsymbol{t}}} \hat{\boldsymbol{t}} = |\hat{\boldsymbol{s}}| \cos \theta_v \, \hat{\boldsymbol{s}}_v$$

If we rearrange the sum of rejection components:

$$\boldsymbol{r}_f + \boldsymbol{r}_p = \hat{\boldsymbol{s}} - \frac{\hat{\boldsymbol{s}} \cdot \hat{\boldsymbol{t}}}{\hat{\boldsymbol{t}} \cdot \hat{\boldsymbol{t}}} \hat{\boldsymbol{t}}$$

To be:

$$\boldsymbol{r}_p + \frac{\hat{\boldsymbol{s}} \cdot \hat{\boldsymbol{t}}}{\hat{\boldsymbol{t}} \cdot \hat{\boldsymbol{t}}} \hat{\boldsymbol{t}} = \hat{\boldsymbol{s}} - \boldsymbol{r}_f$$

We can apply it as such:

$$\hat{\boldsymbol{s}} - \boldsymbol{r}_f = |\hat{\boldsymbol{s}}| \cos \theta_v \, \hat{\boldsymbol{s}}_v$$

Next, if we take the magnitudes of both sides:

$$\left| \hat{\boldsymbol{s}} - \boldsymbol{r}_f \right| = \left| |\hat{\boldsymbol{s}}| \cos \theta_v \, \hat{\boldsymbol{s}}_v \right|$$

Since $\hat{\boldsymbol{s}}$ and $\hat{\boldsymbol{s}}_v$ are both unit vectors, the following equation for the varus angle can be obtained:

$$\cos \theta_v = \left| \hat{\boldsymbol{s}} - \boldsymbol{r}_f \right| \tag{35}$$

Note that this requires the varus angle to be between -90 and 90 degrees. $\boldsymbol{r}_f$ can be described using the rejection $\boldsymbol{r}$, as well as the flexion axis $\hat{\boldsymbol{f}}$.

$$\hat{\boldsymbol{f}} = \hat{\boldsymbol{t}} \times \hat{\boldsymbol{t}}_p \tag{36}$$

$$\boldsymbol{r}_f = \frac{\boldsymbol{r} \cdot \hat{\boldsymbol{f}}}{\hat{\boldsymbol{f}} \cdot \hat{\boldsymbol{f}}} \hat{\boldsymbol{f}} \tag{37}$$

F3.1.2. Determining Varus Rotation Sign

The arccosine function does not distinguish between positive and negative angles, so the sign of the varus angle must be determined in another way. Given that the flexion axis always points towards the participant's right, the sign of the dot product of $\hat{\boldsymbol{f}}$ and $\boldsymbol{r}_f$ informs us whether the shank was rotated medially or laterally with respect to the thigh. The sign was determined for the participant's right leg as below:

$$varus\ sign = \begin{cases} -1, & \hat{\boldsymbol{f}} \cdot \boldsymbol{r}_f \geq 0 \\ +1, & \hat{\boldsymbol{f}} \cdot \boldsymbol{r}_f < 0 \end{cases} \quad (38)$$

F3.2. Flexion

F3.2.1. Determining Flexion Magnitude

The equation for applying a rotation vector with an axis of $\hat{\boldsymbol{t}}_{pf}$ and an angle of θ_v to a vector $\hat{\boldsymbol{t}}_f$ is:

$$\hat{\boldsymbol{s}} = (cos\theta_v)\hat{\boldsymbol{t}}_f + (\sin\theta_v)\left(\hat{\boldsymbol{t}}_{pf} \times \hat{\boldsymbol{t}}_f\right) + (1 - \cos\theta_v)\left(\hat{\boldsymbol{t}}_{pf} \cdot \hat{\boldsymbol{t}}_f\right)\hat{\boldsymbol{t}}_{pf}$$

The angle θ_v is the signed varus angle found earlier. The vector $\hat{\boldsymbol{t}}_f$ undergoing rotation is the "flexed thigh," obtained by rotating $\hat{\boldsymbol{t}}$ about $\hat{\boldsymbol{f}}$ by the amount of flexion present. Rotating $\hat{\boldsymbol{t}}_p$ in this same fashion gives the axis $\hat{\boldsymbol{t}}_{pf}$, which effectively functions as a varus axis.

While many of these terms are unknown, they can be described using a series of identities. The cross product of the "flexed" thigh and thigh perpendicular vectors is the same as that of the original thigh and thigh perpendicular vectors. This cross product is equivalent to the flexion axis, and since both $\hat{\boldsymbol{t}}_f$ and $\hat{\boldsymbol{t}}_{pf}$ were obtained through rotation by the same angle about this axis, the result is the same.

$$\hat{\boldsymbol{t}}_{pf} \times \hat{\boldsymbol{t}}_f = \hat{\boldsymbol{t}}_p \times \hat{\boldsymbol{t}}$$

Since the "flexed" thigh and its respective perpendicular vector are perpendicular, their dot product is zero.

$$\hat{\boldsymbol{t}}_{pf} \cdot \hat{\boldsymbol{t}}_f = 0$$

Application of both of these identities yields:

$$\hat{\boldsymbol{s}} = (cos\theta_v)\hat{\boldsymbol{t}}_f + (\sin\theta_v)\left(\hat{\boldsymbol{t}}_p \times \hat{\boldsymbol{t}}\right)$$

Now we can solve for the "flexed" thigh:

$$\hat{\boldsymbol{s}} - (\sin\theta_v)\left(\hat{\boldsymbol{t}}_p \times \hat{\boldsymbol{t}}\right) = (cos\theta_v)\hat{\boldsymbol{t}}_f$$

$$\hat{\boldsymbol{t}}_f = \frac{\hat{\boldsymbol{s}} - (\sin\theta_v)\left(\hat{\boldsymbol{t}}_p \times \hat{\boldsymbol{t}}\right)}{(cos\theta_v)} \quad (39)$$

Note that this equation becomes unstable if the varus angle approaches -90 or 90 degrees. Both of these extremes are far outside of what occurs during normal gait (Leardini et al., 2005; LaFortune et al., 1992).

Now, the flexion angle is simply the angle between $\hat{\boldsymbol{t}}$ and $\hat{\boldsymbol{t}}_f$.

$$\cos\theta_f = \frac{\hat{\boldsymbol{t}}_f \cdot \hat{\boldsymbol{t}}}{|\hat{\boldsymbol{t}}_f||\hat{\boldsymbol{t}}\,|} \tag{40}$$

F3.2.2. Determining Flexion Sign

Consider the "flexed" thigh $\hat{\boldsymbol{t}}_f$ again. Under positive knee flexion, this vector points towards the rear of the body. Thus, the dot product of this vector and the thigh's perpendicular vector would be negative in the presence of positive knee flexion. The sign of the flexion rotation is:

$$flexion\ sign = \begin{cases} -1, & \hat{\boldsymbol{t}}_f \cdot \hat{\boldsymbol{t}}_p \geq 0 \\ +1, & \hat{\boldsymbol{t}}_f \cdot \hat{\boldsymbol{t}}_p < 0 \end{cases} \tag{41}$$

F3.3. Internal Rotation

F3.3.1. Determining Internal Rotation Magnitude

First apply the flexion and varus rotations to the thigh's perpendicular vector to create $\hat{\boldsymbol{t}}_{pfv}$. This new vector is associated with a thigh that is very nearly collinear with the shank. The angle between this adjusted perpendicular vector and the shank's perpendicular vector is the internal rotation.

$$\cos\theta_i = \frac{\hat{\boldsymbol{t}}_{pfv} \cdot \hat{\boldsymbol{s}}_p}{|\hat{\boldsymbol{t}}_{pfv}||\hat{\boldsymbol{s}}_p|} \tag{42}$$

F3.3.2. Determining Internal Rotation Sign

Attempting to rotate $\hat{\boldsymbol{t}}_{pfv}$ about the shank should, if done correctly, give a vector very nearly identical to $\hat{\boldsymbol{s}}_p$. Given the downward direction of the shank vector, applying a positive angle rotates the vector outwards. If this makes this new perpendicular vector line up with the shank's perpendicular vector, then the internal rotation's sign is negative. If not, then the rotation's sign is positive.

$$internal\ sign = \begin{cases} -1, & |\hat{\boldsymbol{t}}_{pfvi} - \hat{\boldsymbol{s}}_p| < 10^{-8} \\ +1, & |\hat{\boldsymbol{t}}_{pfvi} - \hat{\boldsymbol{s}}_p| \geq 10^{-8} \end{cases} \tag{43}$$